Article

Cell

AgRP Neurons Control Systemic Insulin Sensitivity via Myostatin Expression in Brown Adipose Tissue

Graphical Abstract

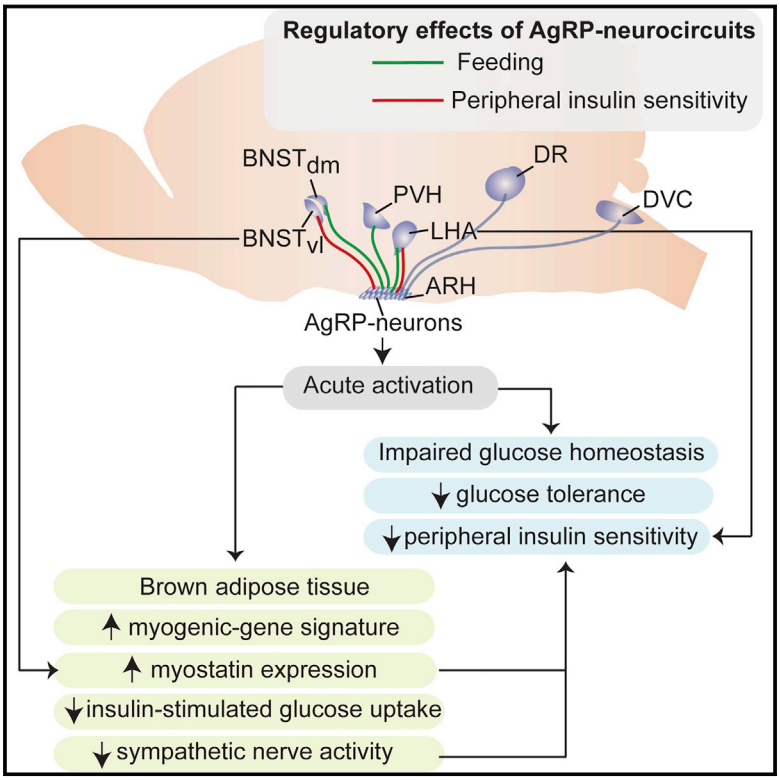

Highlights

- Acute activation of AgRP neurons stimulates *myostatin* expression in BAT
- AgRP neuron activity-induced *myostatin* expression impairs insulin sensitivity
- AgRP neuron activation decreases BAT sympathetic nerve activity and glucose uptake
- Distinct and overlapping AgRP neurocircuits control insulin sensitivity and feeding

Authors

Sophie M. Steculorum, Johan Ruud, Ismene Karakasilioti, ..., F. Thomas Wunderlich, Peter Kloppenburg, Jens C. Brüning

Correspondence

bruening@sf.mpg.de

In Brief

Neural circuits containing AgRP neurons coordinate hunger states with glucose homeostasis by inducing, in addition to eating, insulin resistance via stimulating expression of muscle-related genes in brown adipose tissue that inhibit glucose uptake.

Accession Numbers

GSE77766

Steculorum et al., 2016, Cell *165*, 125–138
March 24, 2016 ©2016 Elsevier Inc.
http://dx.doi.org/10.1016/j.cell.2016.02.044

Article

Cell

AgRP Neurons Control Systemic Insulin Sensitivity via Myostatin Expression in Brown Adipose Tissue

Sophie M. Steculorum,[1,2,3,9] Johan Ruud,[1,2,3,9] Ismene Karakasilioti,[1,2,3] Heiko Backes,[1,2,3] Linda Engström Ruud,[1,2,3] Katharina Timper,[1,2,3] Martin E. Hess,[1,2,3] Eva Tsaousidou,[1,2,3] Jan Mauer,[1,2,3] Merly C. Vogt,[1,2,3] Lars Paeger,[3,4] Stephan Bremser,[3,4] Andreas C. Klein,[3,4] Donald A. Morgan,[5] Peter Frommolt,[3] Paul T. Brinkkötter,[3,6] Philipp Hammerschmidt,[1] Thomas Benzing,[3,6] Kamal Rahmouni,[5,7] F. Thomas Wunderlich,[1,2,3] Peter Kloppenburg,[3,4] and Jens C. Brüning[1,2,3,8,*]

[1]Department of Neuronal Control of Metabolism, Max Planck Institute for Metabolism Research, Gleueler Strasse 50, 50931 Cologne, Germany

[2]Center for Endocrinology, Diabetes and Preventive Medicine (CEDP), University Hospital Cologne, Kerpener Strasse 26, 50924 Cologne, Germany

[3]Excellence Cluster on Cellular Stress Responses in Aging Associated Diseases (CECAD) and Center for Molecular Medicine Cologne (CMMC), University of Cologne, Joseph-Stelzmann-Strasse 26, 50931 Cologne, Germany

[4]Biocenter, Institute for Zoology, University of Cologne, Zülpicher Strasse 47b, 50674 Cologne, Germany

[5]Department of Pharmacology, University of Iowa Carver College of Medicine, Iowa City, IA 52242, USA

[6]Department II of Internal Medicine, University Hospital Cologne, Kerpener Strasse 62, 50937 Cologne, Germany

[7]Fraternal Order of Eagles Diabetes Research Center, University of Iowa Carver College of Medicine, Iowa City, IA 55242, USA

[8]National Center for Diabetes Research (DZD) Ingolstädter Land Strasse 1, 85764 Neuherberg, Germany

[9]Co-first author

*Correspondence: bruening@sf.mpg.de

http://dx.doi.org/10.1016/j.cell.2016.02.044

SUMMARY

Activation of Agouti-related peptide (AgRP) neurons potently promotes feeding, and chronically altering their activity also affects peripheral glucose homeostasis. We demonstrate that acute activation of AgRP neurons causes insulin resistance through impairment of insulin-stimulated glucose uptake into brown adipose tissue (BAT). AgRP neuron activation acutely reprograms gene expression in BAT toward a myogenic signature, including increased expression of *myostatin*. Interference with myostatin activity improves insulin sensitivity that was impaired by AgRP neurons activation. Optogenetic circuitry mapping reveals that feeding and insulin sensitivity are controlled by both distinct and overlapping projections. Stimulation of AgRP → LHA projections impairs insulin sensitivity and promotes feeding while activation of AgRP → anterior bed nucleus of the stria terminalis $(aBNST)_{vl}$ projections, distinct from AgRP → $aBNST_{dm}$ projections controlling feeding, mediate the effect of AgRP neuron activation on BAT-myostatin expression and insulin sensitivity. Collectively, our results suggest that AgRP neurons in mice induce not only eating, but also insulin resistance by stimulating expression of muscle-related genes in BAT, revealing a mechanism by which these neurons rapidly coordinate hunger states with glucose homeostasis.

INTRODUCTION

Obesity represents a major health burden, currently affecting more than 30% of Western populations and it results from a de-regulated balance between caloric intake and energy expenditure. Energy homeostasis is maintained through hormonal and nutrient feedback signals communicating peripheral fuel availability to the CNS to accordingly adapt behavioral and autonomic responses through the control of energy intake and expenditure (Belgardt and Brüning, 2010). Here, acute regulation of AgRP neurons plays a predominant role in control of feeding, as inducible ablation of these neurons in adult mice leads to immediate cessation of feeding and as acute chemogenetic or optogenetic activation of these neurons provokes voracious feeding (Gropp et al., 2005; Luquet et al., 2005; Aponte et al., 2011; Krashes et al., 2011). Of note, the food intake regulatory function of these neurons is not only mediated through AgRP release, but also by co-release of neuropeptide Y (NPY) and the inhibitory neurotransmitter GABA (Atasoy et al., 2012). According to their fundamental function in control of feeding, AgRP neurons integrate numerous signals from the periphery, which communicate nutrient availability in the organism, including ghrelin, insulin, glucose, and the purine base derivative, UDP (Andrews et al., 2008; Plum et al., 2006; Könner et al., 2007; Parton et al., 2007; Steculorum et al., 2015).

Recent sophisticated optogenetic neurocircuitry mapping experiments have provided important new insights into the neuronal network architecture underlying the control of feeding. Betley et al. (2013) demonstrated that redundant pathways originating from AgRP neurons and projecting to the anterior bed nucleus of the stria terminalis (aBNST), paraventricular hypothalamic nucleus (PVH), lateral hypothalamus (LHA), and paraventricular thalamic nucleus (PVT) mediate AgRP neuron-evoked

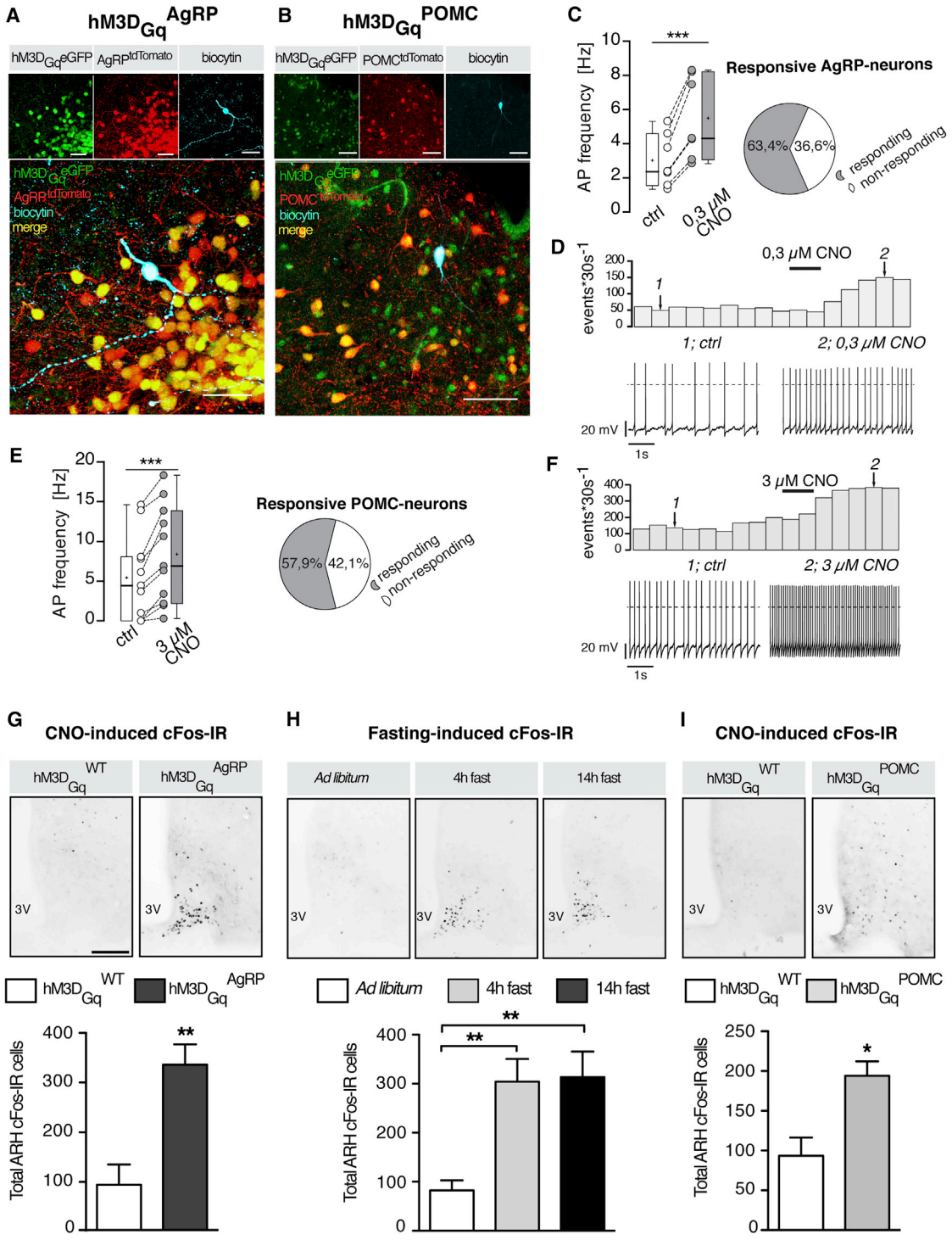

Figure 1. Efficient Transgenic Chemogenetic Activation of AgRP and POMC Neurons

(A and B) Representative microphotographs showing expression of $hM3D_{Gq}$ in (A) AgRP neurons and (B) POMC neurons. Overlay in large panel shows the expression of tdtomato and eGFP in the neuron recorded (biocytin filled). Scale bars, 40 μm.

(C and E) Pie charts represent the ratio between CNO-responsive and non-responsive neurons. (C) Action potential (AP) frequency of responding AgRP neurons (n_{total} = 11: $n_{responding}$ = 7 and $n_{non\text{-}responding}$ = 4), and (E) of responding POMC neurons (n_{total} = 19: $n_{responding}$ = 11 and $n_{non\text{-}responding}$ = 8).

(D and F) Example rate histograms and the respective original recordings of an AgRP neuron and a POMC neuron, respectively. Numbered arrows mark bins of which original traces in the lower panel are extracted.

(legend continued on next page)

stimulation of feeding. Very recently, another characteristic of the homeostatic regulation of feeding governed by AgRP neurons was discovered, where AgRP neurons exhibit properties consistent with a negative-valence teaching signal (Betley et al., 2015).

In addition to their crucial role in controlling feeding, AgRP neurons and the melanocortin circuitry have been implicated in the long-term regulation of peripheral glucose homeostasis (Könner et al., 2007). From an evolutionary point of view, it is reasonable to assume that the same neurons, which control uptake of nutrients from outside the body according to energy state, also control nutrient fluxes across different peripheral organs (Vogt and Brüning, 2013). Along this line, we demonstrated that insulin's ability to inhibit AgRP neuron firing is required for its effect to suppress hepatic glucose production in mice (Könner et al., 2007). Similarly, chronic simultaneous ablation of insulin and leptin receptors from pro-opiomelanocortin (POMC) neurons results in profound deregulation of peripheral glucose metabolism (Hill et al., 2010). In addition, targeted re-expression of the MC4R revealed distinct effector sites for MC4R-dependent control of feeding and chronic regulation of peripheral glucose metabolism (Morgan et al., 2015; Berglund et al., 2014; Balthasar et al., 2005). These studies were, however, all based on models with chronic alterations of signaling systems in AgRP and POMC neurons. Accordingly, it remained undefined whether acute activation of AgRP and POMC neurons exerts acute glucose and insulin sensitivity regulatory effects and if so, which mechanism(s) are involved in this regulation both within the CNS as well as in peripheral organs. Exactly defining the food intake and glucose regulatory functions of these neurons is of critical importance, since obesity-associated hypothalamic inflammation and associated alterations of AgRP neuron activity can contribute to the manifestation of obesity and progression of insulin resistance (Tsaousidou et al., 2014; Kleinridders et al., 2009; Belgardt et al., 2010). Moreover, improved glucose metabolism in high fat diet (HFD)-fed mice upon toxin-mediated ablation of AgRP-neurons further highlights the dependence of metabolic alterations in obesity on the activity of these cells (Joly-Amado et al., 2012).

Therefore, we employed chemogenetic and optogenetic tools to investigate if and how activation of AgRP or POMC neurons affects the short-term regulation of systemic glucose homeostasis. We find that activation of AgRP neurons, but not of POMC neurons, acutely impairs systemic insulin sensitivity. Acute activation of AgRP neurons inhibits insulin-stimulated glucose uptake in BAT, regulates sympathetic nerve activity to BAT, and leads to altered gene expression in BAT with upregulation of a myogenic gene signature, including myostatin. Myostatin-neutralizing antibodies attenuated the insulin resistance-inducing effect of AgRP neuron activation. Employing optogenetic circuitry mapping approaches, we delineate the distinct and overlapping architecture of the neurocircuitry responsible for acute feeding and insulin sensitivity.

RESULTS

Chemogenetic Activation of AgRP Neurons Causes Insulin Resistance

To investigate the effect of activating AgRP neurons on systemic glucose homeostasis and insulin sensitivity, we generated mice that allow for Cre-dependent expression of the stimulatory DREADD-receptors hM3D$_{Gq}$ from the ROSA26-locus (Alexander et al., 2009) (Figure S1A). Crossing these animals with either AgRP^{Cre} or POMC^{Cre} mice yielded successful expression of the transgene in these neurons as evidenced by GFP immunoreactivity of an eGFP cDNA expressed from an internal ribosomal entry site (IRES) downstream of hM3D$_{Gq}$ (Figures 1A, 1B, and S1A).

Electrophysiological recordings revealed potent and fast activation of action potential firing in ~60% of AgRP neurons in ROSA26hM3D$_{Gq}$AgRP mice (hM3D$_{Gq}^{AgRP}$ mice) upon incubating hypothalamic slices with 0.3 μM clozapine-N-oxide (CNO) (Figures 1C and 1D). POMC neurons also elicited action potential firing upon CNO-induced activation of these neurons in hM3D$_{Gq}^{POMC}$ mice (Figures 1E and 1F). However, at the same dose of CNO (0.3 μM), only ~20% of POMC neurons responded with a significant increase in action potential frequency (Figure S1B). When we increased the dose of CNO to 3 μM, ~60% of POMC neurons responded to CNO incubation including some that had not responded to previous application of 0.3 μM CNO (Figures 1E, 1F, and S1B).

In vivo administration of CNO (0.3 mg/kg body weight [BW]) in hM3D$_{Gq}^{AgRP}$ mice evoked a clear enhancement of cFos immunoreactivity in the arcuate nucleus of the hypothalamus (ARH) of these mice, and both the distribution and quantity of cFos-immunoreactive cells was comparable to that observed in the ARH of mice that had been fasted for either 4 or 14 hr (Figures 1G and 1H). Similarly, in vivo administration of CNO (0.3 mg/kg BW) evoked a clear enhancement of cFos immunoreactivity in the ARH of hM3D$_{Gq}^{POMC}$-mice (Figure 1I). To compare the CNO-evoked POMC neuron activation to that observed upon re-feeding, we employed in vivo calcium (Ca^{2+}) photometry in ARH of hM3D$_{Gq}^{POMC}$ mice. Re-feeding resulted in a significant increase in intracellular Ca^{2+} in POMC neurons comparable to that observed upon injection of 0.3 or 3 mg/kg BW of CNO (Figures S1C and S1D). Thus, the CNO doses employed in vivo efficiently activate both AgRP and POMC neurons upon expression of hM3D$_{Gq}$ in these neurons to a comparable extent as observed during their physiological, feeding state-dependent regulation.

Chemogenetic activation of hM3D$_{Gq}$-expressing AgRP neurons potently activated food intake comparable to what

(G–I) CNO-evoked cFos immunoreactivity in the arcuate nucleus (ARH) of (G) h3MD$_{Gq}^{AgRP}$, (I) h3MD$_{Gq}^{POMC}$, and h3MD$_{Gq}^{WT}$ mice. (H) Fasting-induced cFos immunoreactivity in the ARH of C57BL/6 mice subjected to a 4 hr or 14 hr fast or random fed. Images and quantification comparison of cFos immunoreactivity in the ARH following CNO administration (0.3 mg/kg BW; i.p.) in (G) hM3D$_{Gq}^{AgRP}$ mice and hM3D$_{Gq}^{WT}$ mice (n = 3 versus 4), (I) hM3D$_{Gq}^{POMC}$ and hM3D$_{Gq}^{WT}$ mice (n = 4 versus 4), and (H) fasted mice (n = 7–8 in each group) and random fed mice (n = 8). Scale bars, 100 μm. 3V, third ventricle. Data are represented as boxplots and generated according to the "Tukey method" (mean, +; median, horizontal line) (C and E) and as mean ± SEM (G–I). *p ≤ 0.05, **p ≤ 0.01, and ***p ≤ 0.001 as determined by paired Student's t test (C and E) and unpaired Student's t test (G–I).
See also Figure S1B.

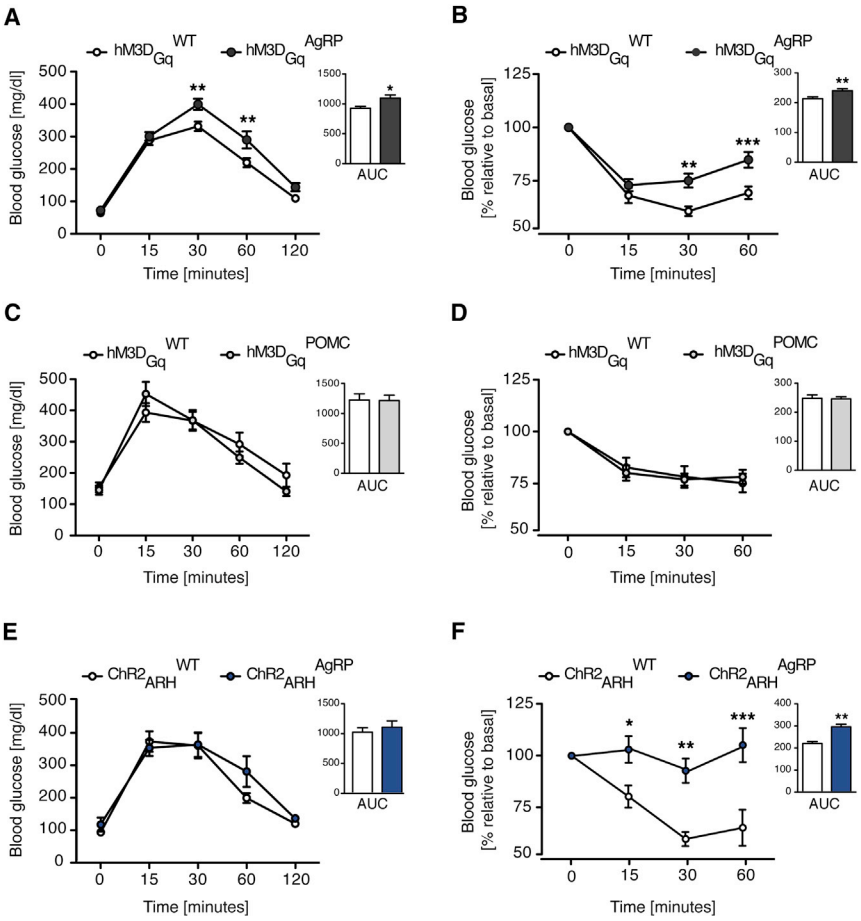

Figure 2. Chemogenetic and Optogenetic Activation of AgRP Neurons Promotes Systemic Insulin Resistance

(A and C) Glucose tolerance test (GTT) performed in (A) hM3D$_{Gq}^{AgRP}$ mice and control mice (n = 14 versus 15) and (C) hM3D$_{Gq}^{POMC}$ mice and control mice (n = 7 versus 7) after clozapine-N-oxide (CNO, 0.3 mg/kg BW;i.p.) administration.

(B and D) Insulin tolerance test (ITT) in (B) hM3D$_{Gq}^{AgRP}$ mice (n = 16 versus 17) and (D) hM3D$_{Gq}^{POMC}$ (n = 10 versus 12) after CNO treatment (0.3 mg/kg BW; i.p.).

(E and F) GTT (n = 8 versus 9) (E) and ITT (n = 8 versus 9) (F) during somatic stimulation of ARH AgRP neurons (ChR2$_{ARH}^{AgRP}$) and control litter mates (ChR2$_{ARH}^{WT}$). Area under the curves (AUC) of each GTT and ITT are plotted next to the corresponding curves. Data are represented as mean ± SEM. *p ≤ 0.05, **p ≤ 0.01, and ***p ≤ 0.001 as determined by two-way ANOVA followed by Bonferroni post hoc test for the curves and unpaired Student's t test for the AUC.

See also Figure S2.

has been published previously (Figure S1E) (Aponte et al., 2011; Krashes et al., 2011). Similarly, AgRP neuron activation in hM3D$_{Gq}^{AgRP}$ mice increased locomotor activity 140 min following CNO injection in the absence of food (Figure S1F) consistent with previous reports (Dietrich et al., 2015; Krashes et al., 2011). Moreover, activation of POMC neurons upon CNO injection of hM3D$_{Gq}^{POMC}$ mice during the dark phase resulted in acute suppression of feeding (Figure S1G). While previous studies reported that only prolonged activation of POMC neurons suppresses feeding (Aponte et al., 2011; Zhan et al., 2013), CNO administration in hM3D$_{Gq}^{POMC}$ mice significantly decreases feeding after 1 hr. This discrepancy can originate from different methodical aspects such as number of neurons activated by the respective approaches. Nevertheless, hM3D$_{Gq}$-dependent chemogenetic activation represents a suitable approach to study the effects of acute activation of AgRP and POMC neurons in vivo.

Next, we investigated the effect of acutely activating AgRP or POMC neurons on peripheral glucose homeostasis and insulin sensitivity by assessing glucose and insulin tolerance after CNO injection to hM3D$_{Gq}^{AgRP}$ and hM3D$_{Gq}^{POMC}$ mice and their littermate controls (Figures S2A and S2B). To avoid any confounding effect of altered food intake, all experiments were performed without providing food to the animals subsequent to CNO injection. We found that injection of CNO in hM3D$_{Gq}^{AgRP}$ mice acutely impaired glucose tolerance and insulin tolerance (Figures 2A and 2B). In contrast, activating POMC neurons in hM3D$_{Gq}^{POMC}$ mice had no effect on either glucose tolerance or insulin sensitivity (Figures 2C and 2D), not even when they were injected with 3 mg/kg BW of CNO or upon prolonged application of CNO 16 hr prior to the GTT (Figures S2C–S2E). We further employed a complimentary approach by optogenetically activating AgRP neurons (Figures S2F and S2G). Therefore, we crossed mice allowing for Cre-dependent expression of channelrhodopsin 2 (ChR2) (Madisen et al., 2012) with AgRP-Cre mice to yield ChR2^{AgRP} animals and AgRP^{Cre}-negative control littermates (ChR2^{WT}) (Figure S2H). Unilateral optogenetic activation of AgRP neurons in the ARH of these mice resulted in pronounced induction of feeding as previously reported (Aponte et al., 2011) (Figure S2I). Moreover, optogenetic activation of AgRP neurons in ChR2^{AgRP} mice induced severe insulin resistance, without affecting glucose tolerance (Figures 2E and 2F).

Activation of AgRP Neurons Impairs Insulin-Stimulated Glucose Uptake in BAT

To define which aspect of peripheral glucose homeostasis is modulated upon acute activation of AgRP neurons, we performed euglycemic-hyperinsulinemic clamps in hM3D$_{Gq}^{AgRP}$ and control mice (Figure S3A). To circumvent any potentially confounding effect of altered locomotor activity following AgRP neuron activation, the clamp studies were performed in restrained animals. While both groups of mice achieved the same degree of glycemia during the steady-state phase of the clamp (Figure S3B), the glucose infusion rate (GIR) required to

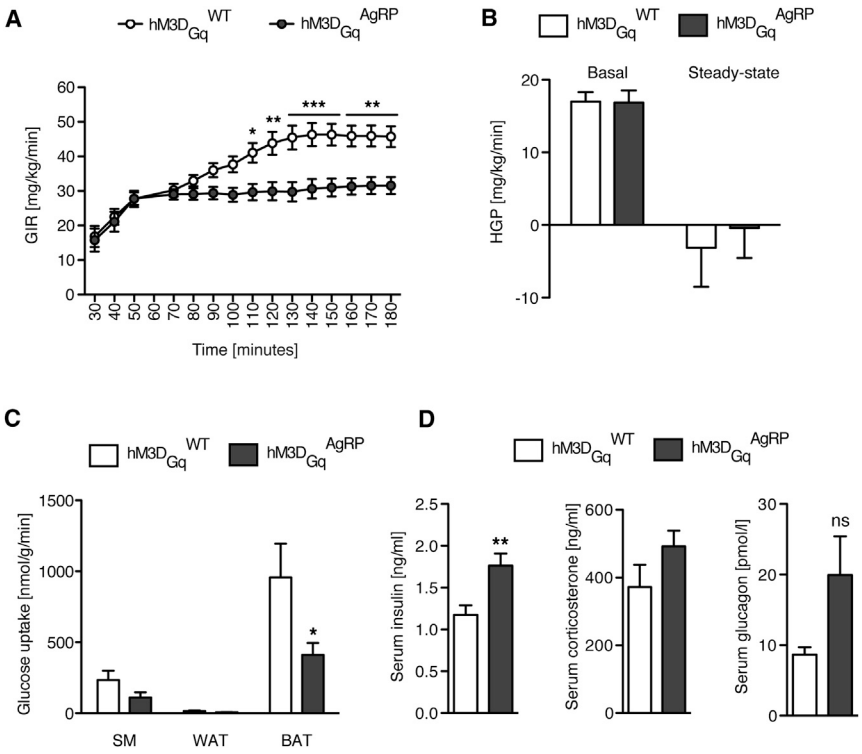

Figure 3. Chemogenetic Activation of AgRP Neurons Inhibits BAT Glucose Uptake

(A) Glucose infusion rates (GIR) during the euglycemic-hyperinsulinemic clamp in hM3D$_{Gq}^{WT}$ control littermates and hM3D$_{Gq}^{AgRP}$ mice (n = 23 versus 20).

(B) Hepatic glucose production (HGP) measured under basal and steady-state conditions during the clamp (n = 23 versus 20).

(C) Tissue-specific insulin-stimulated glucose uptake rates in skeletal muscle (SM), white adipose tissue (WAT), and brown adipose tissue (BAT) (n = 23 versus 18–19).

(D) Serum insulin, corticosterone, and glucagon levels of hM3D$_{Gq}^{AgRP}$ and hM3D$_{Gq}^{WT}$ 1 hr post CNO administration (n = 10 versus 10). All data are represented as mean ± SEM. *p ≤ 0.05, **p ≤ 0.01, and ***p ≤ 0.001 as determined by two-way ANOVA followed by Bonferroni post hoc test (A), one-tailed unpaired Student's t test (C), and two-tailed unpaired Student's t test (D).

maintain euglycemia was significantly reduced in hM3D$_{Gq}^{AgRP}$ mice (Figure 3A).

When we assessed hepatic glucose production (HGP), hM3D$_{Gq}^{AgRP}$ and control mice exhibited no significant differences in baseline or in insulin-suppressed rate of HGP (Figure 3B). In contrast, insulin's ability to promote glucose uptake into brown adipose tissue (BAT) was significantly reduced by 50% upon AgRP neuron activation, while it remained unaltered in white adipose tissue (WAT) and skeletal muscle (Figure 3C). Additionally, under non-clamp conditions, acute activation of AgRP neurons increased serum insulin concentrations 1 hr after CNO injection, but did not significantly modulate glucagon or corticosterone levels (Figure 3D). Thus, acutely activating AgRP neurons primarily impairs systemic insulin sensitivity via inhibition of insulin-stimulated glucose uptake in BAT. Consistent with this finding, insulin-stimulated BAT glucose uptake is also reduced in obese, HFD-fed mice, in which AgRP neuron activity is chronically altered (Belgardt and Brüning, 2010) (Figures S3G–S3I).

In contrast to hM3D$_{Gq}^{AgRP}$ mice, CNO treatment of hM3D$_{Gq}^{POMC}$ mice had no effect on GIR, tissue-specific glucose uptake rates or insulin's ability to suppress HGP during euglycemic-hyperinsulinemic clamps (Figures S3C–S3F). Thus, acute activation of AgRP neurons, but not POMC neurons, affects systemic glucose metabolism and insulin sensitivity.

Activation of AgRP Neurons Promotes a Myogenic Gene Expression Profile in BAT

Since acute activation of AgRP neurons lead to inhibition of BAT glucose uptake, we asked whether this effect was accompanied by acute changes in gene expression, which could point to the mechanism(s) underlying the development of insulin resistance. We therefore performed a gene expression analysis on BAT-RNA of control and ChR2^{AgRP} mice that had been photo-stimulated in the ARH (ChR2$_{ARH}^{AgRP}$) for 1 hr. This analysis revealed 192 significantly differentially regulated genes (±1.5-fold; $p < 0.005$) in BAT of these mice (Figure 4A; Table S1). Interestingly, gene ontology enrichment analysis revealed an overrepresentation of genes associated with myocyte differentiation and muscle function (Figure 4B; Table S2). In fact, out of 162 upregulated genes, 33 where annotated as muscle-associated transcripts. Interestingly, one of the strongest upregulated genes was myostatin (*Mstn*), which expression was increased by 18-fold upon somatic photostimulation of AgRP neurons (Table S1).

To further validate the increased *myostatin* mRNA expression in BAT after optogenetic activation of AgRP neurons, we assessed its mRNA expression and that of other muscle-associated candidate genes identified in the microarray analysis in BAT of control and hM3D$_{Gq}^{AgRP}$ mice 1 hr following CNO application. This analysis confirmed profound AgRP neuron activation-dependent transcriptional upregulation of *myostatin* and *ankyrin repeat and SOCS box-containing 15* (*Asb15*) (Figure 4C). Moreover, consistent with the effect of AgRP neuron activation to only inhibit glucose uptake in BAT, *myostatin* mRNA expression was found to be increased in BAT following chemogenetic activation of AgRP neurons, but not in skeletal muscle or white adipose tissue depots (Figure S4A). To further investigate whether the effect of optogenetic or chemogenetic activation of AgRP-neurons on BAT *myostatin* mRNA expression reflected a physiological, feeding state-dependent regulation, we next compared *myostatin* expression in BAT of mice that were either feeding randomly or fasted for 14 hr, a state at which AgRP neurons are physiologically activated (Figure 1H). This analysis revealed an upregulation of BAT *myostatin* expression in fasted

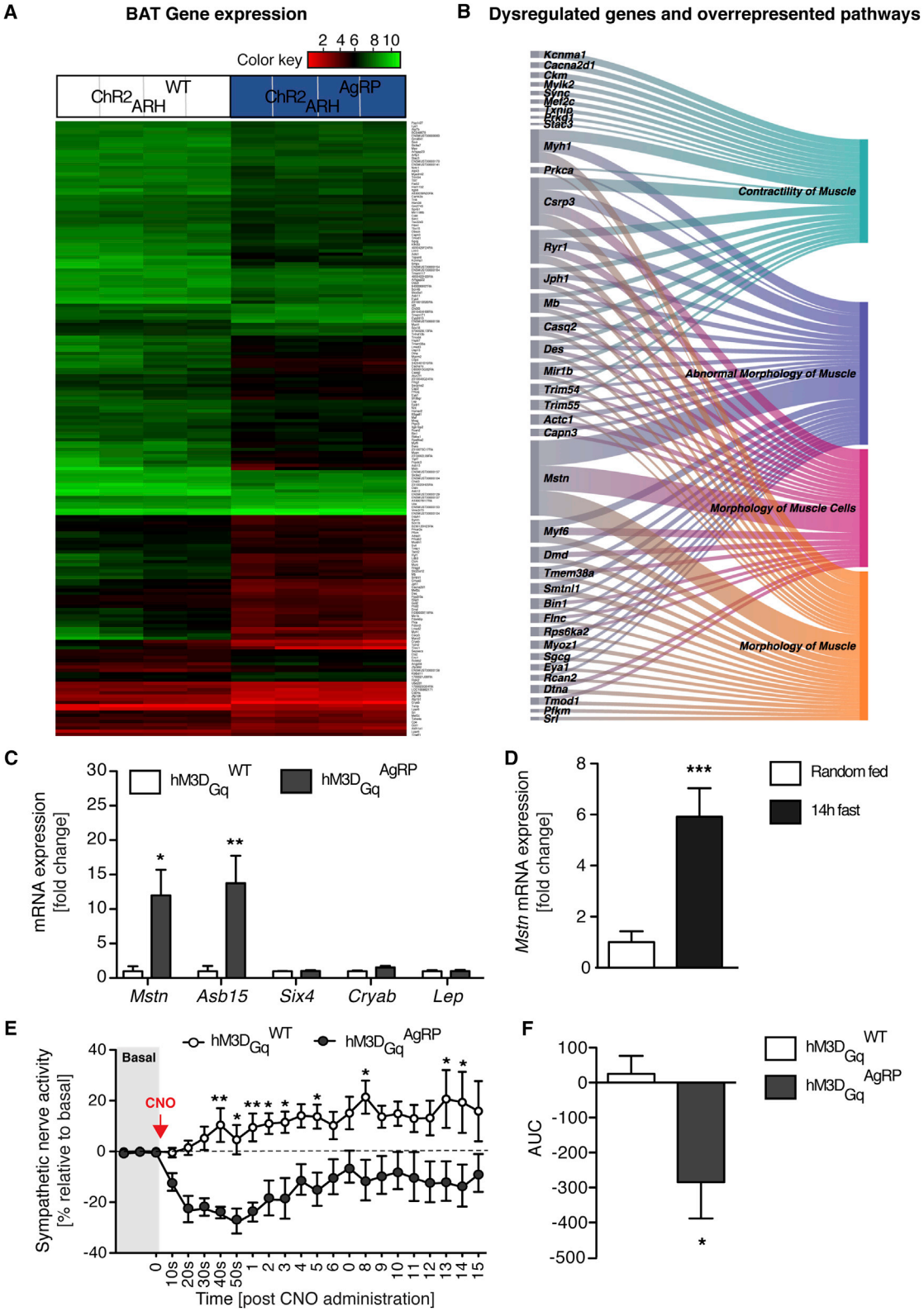

(legend on next page)

mice (Figure 4D). To further address whether AgRP neuron activation not only increases BAT *myostatin* expression but also circulating myostatin levels, we assessed myostatin concentrations in serum of control and $hM3D_{Gq}^{AgRP}$ mice 1 hr following CNO application. Circulating myostatin concentrations increased by ≈20% in mice with activated AgRP neurons compared to controls (Figure S4B). In contrast, *myostatin* mRNA expression remained unaltered in $hM3D_{Gq}^{POMC}$ mice (Figure S4C).

Interestingly, BAT-precursor cells originate from a Myf-5-positive lineage, which can give rise either to myocytes or brown adipocytes and β adrenergic stimulation can potently direct their gene expression profile and differentiation toward the brown adipocyte lineage (Kajimura et al., 2009; Seale et al., 2008; Timmons et al., 2007). Thus, the profoundly and coordinately deregulated gene expression profile in BAT toward a myogenic signature together with the pre-described reduction in energy expenditure in mice upon chemogenetic AgRP neuron activation may point toward reduced sympathetic activation of BAT upon AgRP neuron activation (Krashes et al., 2011). Thus, we directly recorded BAT sympathetic nerve activity (SNA) in control and $hM3D_{Gq}^{AgRP}$ mice following intravenous injection of CNO. BAT SNA was rapidly suppressed following chemogenetic activation of AgRP neurons (Figures 4E and 4F). Next, we investigated whether the suppression of BAT SNA upon chemogenetic AgRP cell activation could contribute to the insulin resistance-inducing effect of activating these neurons. When we compared the blood glucose-lowering effect of insulin in CNO-treated control and $hM3D_{Gq}^{AgRP}$ mice, which had been either injected with saline or a β3 agonist prior to the insulin tolerance test (ITT), pre-treatment with the β3 agonist abrogated the ability of AgRP neuron activation to impair systemic insulin sensitivity (Figure 5A). These experiments clearly indicate that AgRP neuron activation-dependent suppression of BAT SNA functionally contributes to the development of systemic insulin resistance upon AgRP neuron activation.

Myostatin deficiency enhances BAT differentiation and function and protects from HFD- and high glucose-induced insulin resistance in myocytes (Braga et al., 2013; Kim et al., 2012; Zhang et al., 2011), and myostatin acutely blunts insulin signaling in cultured myocytes and hepatocytes (Bonala et al., 2014). To assess whether myostatin can also induce insulin resistance in brown adipocytes, we investigated the effect of incubating cultured immortalized brown adipocytes with increasing doses of myostatin on insulin-evoked AKT phosphorylation. This analysis revealed that pre-incubation with recombinant myostatin suppressed insulin's ability to promote AKT phosphorylation in parallel to its ability to activate SMAD2/3 phosphorylation (Figures 5B and 5C).

Next, we compared the ability of AgRP neuron activation to impair insulin sensitivity during an ITT in $hM3D_{Gq}^{AgRP}$ mice pretreated with a myostatin-blocking antibody (Ab) or an isotype control immunoglobulin (Smith et al., 2015). IgG treatment had no effect on AgRP neuron-mediated insulin resistance upon CNO injection in $hM3D_{Gq}^{AgRP}$ mice (Figure 5D). However, while injection of the myostatin Ab did not affect insulin tolerance in CNO-treated control mice, it attenuated the ability of CNO-dependent AgRP neuron activation to impair systemic insulin sensitivity (Figure 5D). Thus, our experiments indicate that AgRP neuron-dependent activation of myostatin expression significantly contributes to the manifestation of systemic insulin resistance.

In Vivo Identification of Neurons Activated Downstream of AgRP Neuron Activation

To investigate the neurocircuitry underlying AgRP neuron activation-evoked impairment of systemic insulin sensitivity and myostatin expression in BAT, we employed ^{18}fluoro-deoxyglucose (FDG) positron emission tomography (PET) scanning in order to identify in vivo, which brain areas exhibit altered ^{18}FDG accumulation as a readout for neuronal activation in response to chemogenetic AgRP neuron activation. A significant activation pattern was observed in CNO-treated $hM3D_{Gq}^{AgRP}$ mice in regions consistent with previously described projections of AgRP neurons, including the mediobasal hypothalamus, the LHA, the bed nucleus of the striae terminalis (BNST), raphe nuclei, nucleus accumbens, the parabrachial nucleus (PBN), the periaqueductal gray (PAG), the brainstem (Figures S5A–S5F), and in regions that are less well-appreciated as direct AgRP neuron projection sites such as the motor cortex and cingulate cortex, the somatosensory cortex, as well as the hippocampus (Figures S5G–S5L). While the major advantage of PET-based activity mapping clearly stems from the fact that it allows to assess neuronal activation in vivo, PET scans have limited spatial resolution of ~300 μm.

Thus, we complemented the PET-based analysis of neuronal networks activated in response to AgRP neuron activation through systematic assessment of cFos immunoreactivity. Induction of cFos expression was observed in the PVH, LHA, aBNST as well as the dorsal raphe nucleus in $hM3D_{Gq}^{AgRP}$ (Figures S6A–S6E). Thus, this analysis confirmed the activation pattern of neurons activated downstream of AgRP neurons as

Figure 4. Activation of AgRP Neurons Decreases Sympathetic Nerve Activity to BAT and Acutely Reprograms BAT Gene Expression toward a Myogenic Signature

(A) Heat map of differentially expressed transcripts in the brown adipose tissue (BAT) of $ChR2^{WT}$ versus $ChR2^{AgRP}$ mice (n = 4 mice per group) from photostimulating AgRP neurons for 1 hr, assessed with a cut-off of a change in expression of 1.5-fold and a p value <0.005.

(B) Sankey diagram showing overrepresented pathways on a subset of data presented in (A) in which the width of the arrows is proportional to the fold change.

(C) qRT-PCR analysis of *Myostatin* (*Mstn*), *Ankyrin repeat* and *SOCS box-containing 15* (*Asb15*), *Sine oculis-related homeobox 4* (*Six4*), *crystallin alpha B (Cryab*), and *Leptin* (*Lep*) mRNA expression in the BAT of $hM3D_{Gq}^{AgRP}$ and $hM3D_{Gq}^{WT}$ mice 1 hr after CNO injection (n = 8 versus 10).

(D) qRT-PCR analysis of *Myostatin* (*Mstn*) in the BAT of mice fasted for 14 hr or random fed (n = 5 fasted versus 8 random fed). Mice were killed by decapitation and the BAT harvested 2–3 hr into the dark cycle.

(E) BAT sympathetic nerve recordings at baseline, and time course changes of BAT SN activity after CNO administration from baseline of $hM3D_{Gq}^{AgRP}$ and $hM3D_{Gq}^{WT}$ mice (n = 7 versus 12). Data are represented as mean ± SEM. *p ≤ 0.05, **p ≤ 0.01, and ***p ≤ 0.001 as determined by unpaired Student's t test (C, D and F) and, two-way ANOVA followed by Bonferroni post hoc test for BAT SNA recordings (E).

See also Figure S4 and Tables S1 and S2.

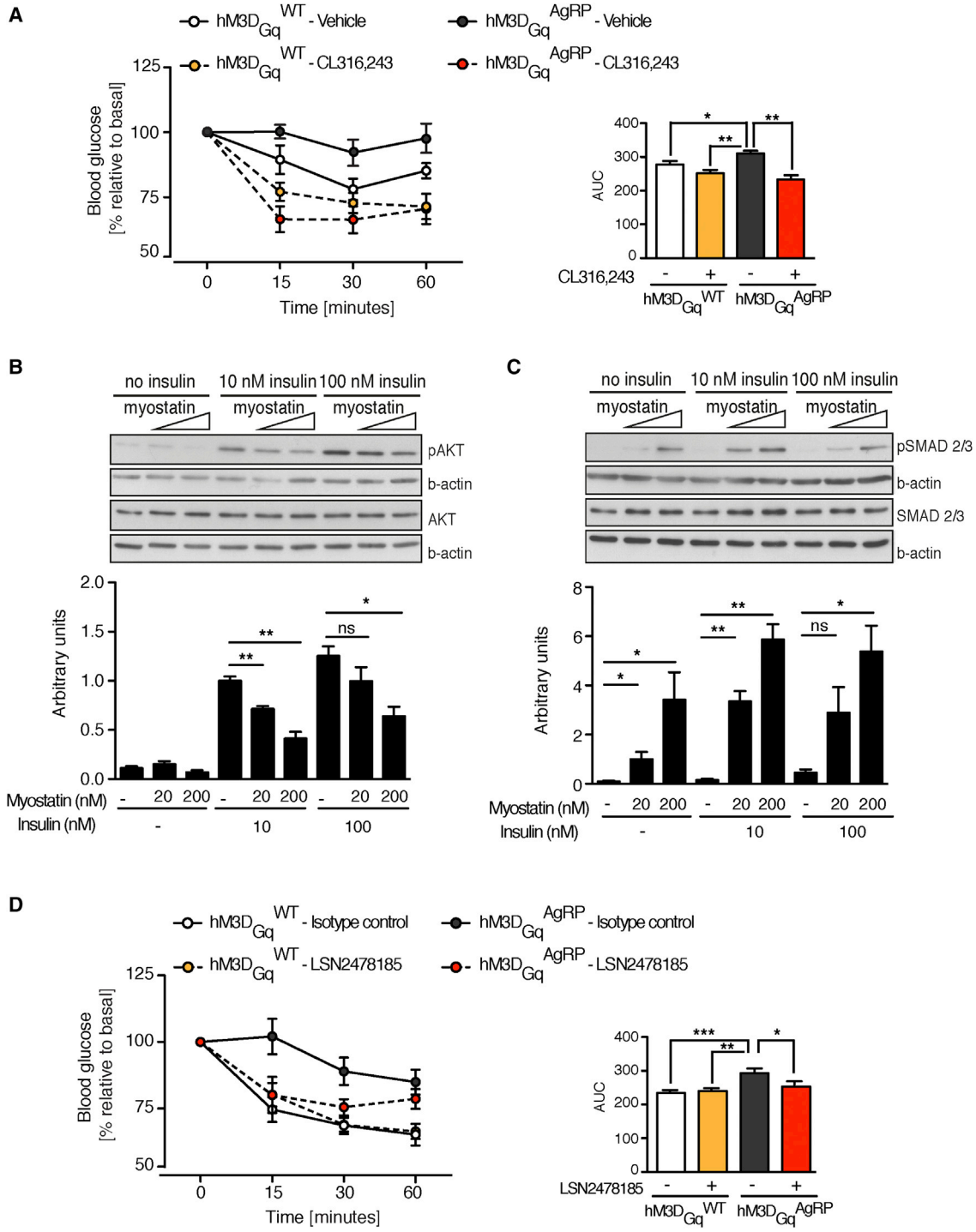

Figure 5. Elevated BAT Myostatin Expression Promotes Insulin Resistance

(A) Insulin tolerance test in hM3D$_{Gq}^{AgRP}$ and hM3D$_{Gq}^{WT}$ mice (n = 7 versus 10) following co-injection of a selective β3-adrenergic agonist (CL 316,243) and CNO, or CNO and vehicle (saline).

(B and C) Representative blots and quantification of pAKT (B) and pSMAD 2/3 (C) from protein lysates of cultured, immortalized brown adipocytes treated with recombinant myostatin in the presence, or absence, of exogenous insulin at the indicated concentrations (n = 3–4 independent experiments).

(D) Insulin tolerance test in CNO-treated hM3D$_{Gq}^{AgRP}$ and hM3D$_{Gq}^{WT}$ mice 12 hr following subcutaneous injection of myostatin neutralizing antibodies (LSN2478185) or isotype control (n = 7 versus 10 for each treatment). Data are represented as mean ± SEM. *p ≤ 0.05, **p ≤ 0.01, and ***p ≤ 0.001 as determined by one-way ANOVA followed by Newman-Keuls post hoc test.

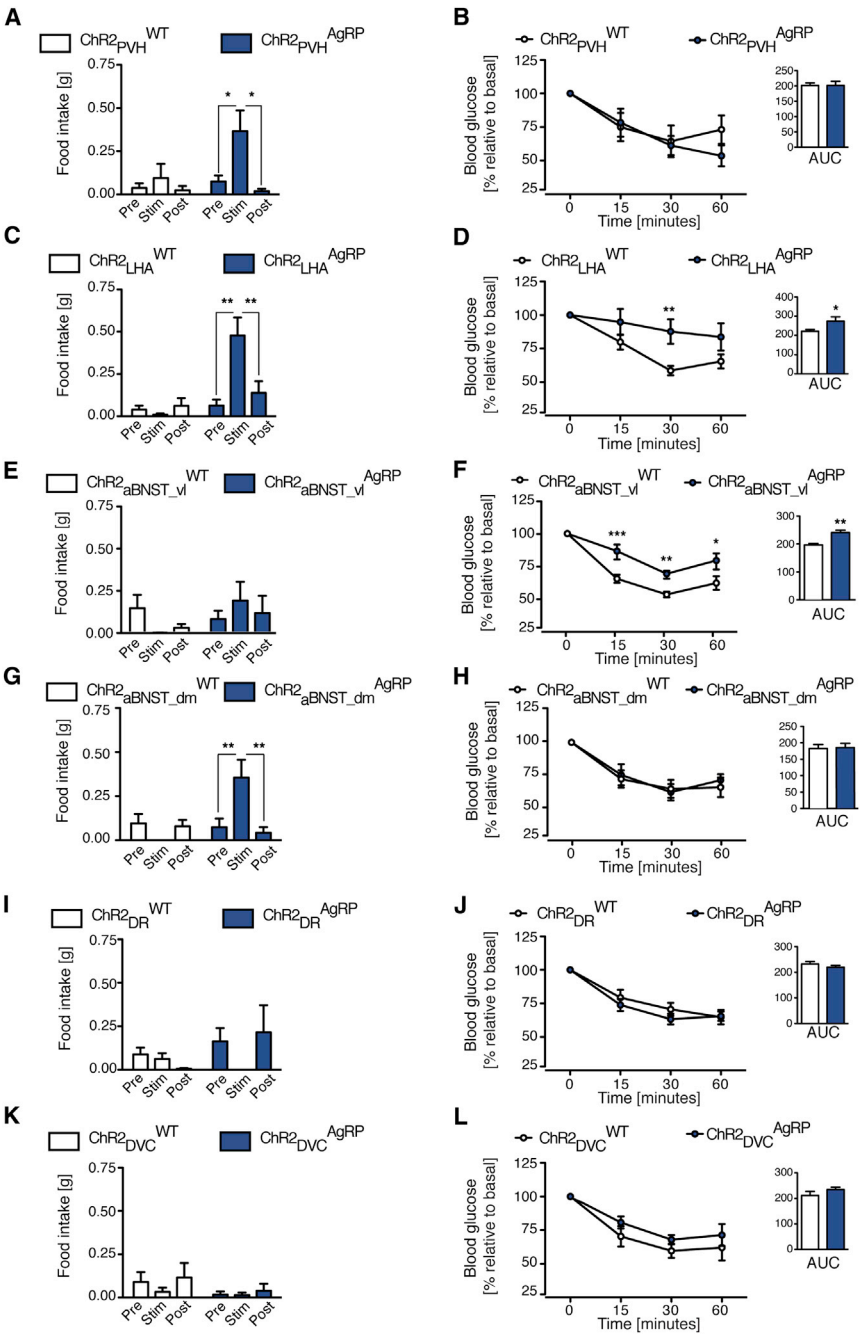

Figure 6. AgRP → LHA and AgRP → aBNST_vl Projections Control Peripheral Insulin Sensitivity

Food intake before (pre), during (stim), and after (post) photostimulation (1 hr per period) and insulin tolerance test (ITT) and respective area under the curve (AUC) in ChR2^{AgRP} mice and ChR2^{WT} mice laser-light stimulated in the following AgRP neuron projection sites: (A and B) the paraventricular nucleus of the hypothalamus (PVH) (n = 7 versus 6); (C and D) the lateral hypothalamic area (LHA) (n = 14 versus 11–13); (E and F) the ventro-lateral anterior bed nucleus of the stria terminalis (aBNST$_{vl}$) (n = 10 versus 9); (G and H) the dorso-medial part of the anterior bed nucleus of the stria terminalis (aBNST$_{dm}$) (n = 11 versus 9); (I and J) the dorsal raphe nucleus (DR) (n = 8–9 versus 6); and (K and L) the dorsal vagal complex (DVC) (n = 6–7 versus 5–6). Data are represented as mean ± SEM. *p ≤ 0.05, **p ≤ 0.01, and ***p ≤ 0.001 as determined by one-way ANOVA followed by Newman-Keuls post hoc test for food intake, by two-way ANOVA followed by Bonferroni post hoc test for ITT curves and by unpaired Student's t test for the AUC graphs.

revealed by ^{18}FDG PET imaging in vivo. It should be pointed out that both techniques may also detect indirect changes in neuronal activity as a consequence of activating GABAergic AgRP neurons, such as via inhibition of local inhibitory interneurons.

Distinct AgRP Projections Mediate the Feeding versus Glucose Regulatory Action of AgRP Neurons

To investigate which AgRP projections mediate the acute glucose regulatory action of these neurons, we employed an optogenetic mapping approach in ChR2^{AgRP} mice. To this end, we implanted optical fibers into AgRP neuron projection sites (Figures S7) and compared the effect of stimulating AgRP fibers specifically in these projection sites on food intake and insulin sensitivity as assessed by ITT. Stimulating AgRP → PVH projections revealed light-evoked activation of feeding as previously described (Atasoy et al., 2012; Betley et al., 2013) but failed to impair systemic insulin sensitivity (Figures 6A and 6B). In contrast, activation of AgRP → LHA projections increased feeding but also induced peripheral insulin resistance (Figures 6C and 6D). Interestingly, whereas stimulation of AgRP → aBNST projections in the ventrolateral part of the aBNST (aBNST$_{vl}$) in ChR2^{AgRP} mice did not modulate feeding, it clearly impaired systemic insulin sensitivity (Figures 6E and 6F). When we targeted a more dorsomedial part (aBNST$_{dm}$), photostimulation evoked a 4-fold increase in feeding in comparison to stimulating the same site in control animals but had no effect on insulin sensitivity (Figures 6G and 6H). Thus, our experiments reveal a functional dichotomy of AgRP → aBNST projections in control of food intake and those in control of peripheral insulin sensitivity. On the other hand, stimulating AgRP → dorsal raphe projections (DR), and AgRP → dorsal vagal complex (DVC) projections had no effect on feeding or on systemic insulin sensitivity (Figures 6I–6L).

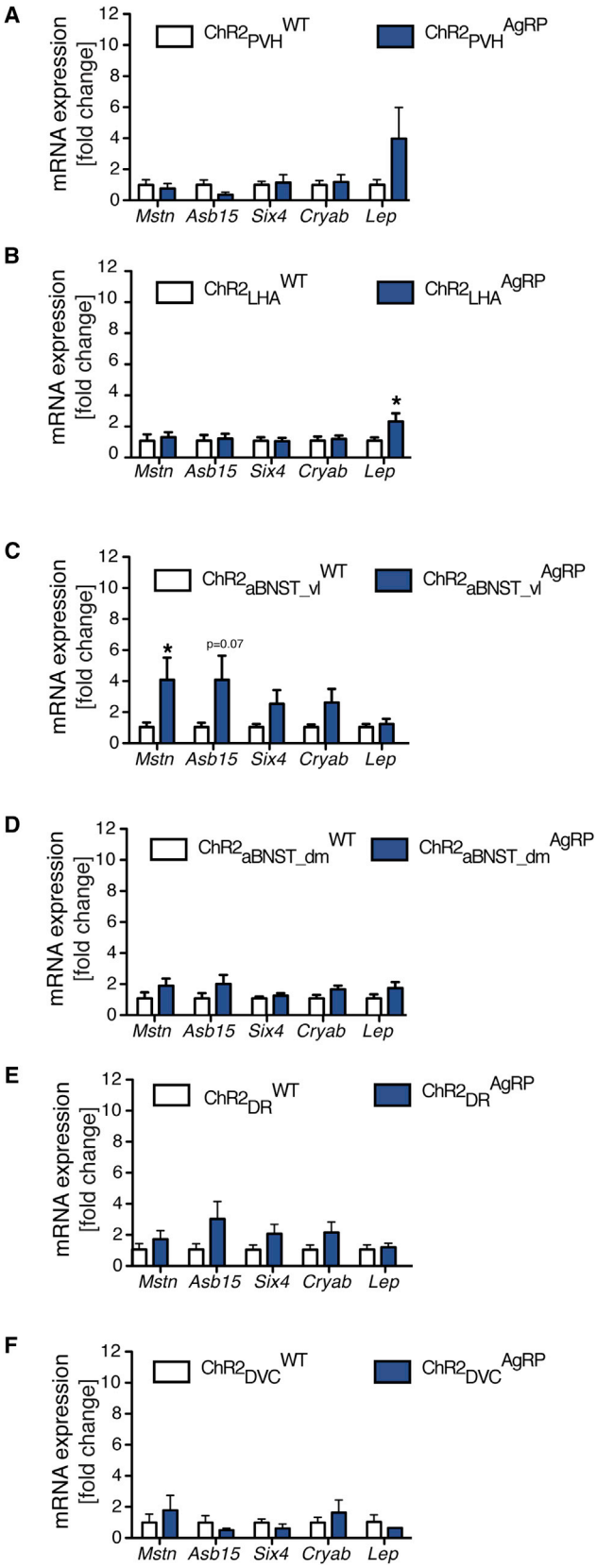

Figure 7. AgRP → aBNST$_{_vl}$ Neurocircuits Mediate the Increase in BAT *Myostatin* Expression

qRT-PCR analysis of *myostatin (Mstn)*, *ankyrin repeat and SOCS box-containing 15 (Asb15)*, *sine oculis-related homeobox 4 (Six4)*, *crystallin alpha B (Cryab)*, and *leptin (Lep)* mRNA expression in the brown adipose tissue of ChR2$_{ARH}^{AgRP}$ mice and ChR2$_{ARH}^{WT}$ mice photostimulated in the following AgRP neuron projection sites: (A) the paraventricular nucleus of the hypothalamus (PVH) (n = 4–6); (B) the lateral hypothalamic area (LHA) (n = 13–9); (C) the ventro-lateral part of the anterior bed nucleus of the stria terminalis (aBNST$_{_vl}$) (n = 10 versus 7); (D) the dorso-medial of the anterior bed nucleus of the stria terminalis (aBNST$_{_dm}$) (n = 10 versus 9); (E) the dorsal raphe nucleus (DR) (n = 7–6); and (F) the dorsal vagal complex (DVC) (n = 3–6). Data are represented as mean ± SEM. *p ≤ 0.05 as determined by unpaired Student's t test.

AgRP → aBNST$_{_vl}$ Projections Regulate *Myostatin* Expression in BAT

Since activation of AgRP → LHA and AgRP → aBNST$_{_vl}$ projections resulted in insulin resistance, we next investigated whether those AgRP projections are also responsible for inducing *myostatin* mRNA expression in BAT. Therefore, we determined the mRNA expression of *myostatin* in BAT of control and ChR2^{AgRP} mice, in which we stimulated AgRP → LHA, AgRP → aBNST$_{_dm}$, or AgRP → aBNST$_{_vl}$ projections. While activation of AgRP → LHA and AgRP → aBNST$_{_dm}$ projections failed to induce *myostatin* expression in BAT, stimulation of AgRP → aBNST$_{_vl}$ projections resulted in pronounced *myostatin* and *Asb15* expression in BAT (Figures 7B–7D). Moreover, activation of AgRP → PVH, AgRP → DR, and AgRP → DVC projections failed to induce *myostatin* mRNA expression in BAT, consistent with the failure of these projection stimulations to affect systemic insulin sensitivity (Figures 7A, 7E, and 7F).

DISCUSSION

Tight regulation of blood glucose concentrations is essential for the survival of the organism. Accordingly, the brain not only controls food intake and energy expenditure, but also coordinately adapts nutrient fluxes across different organs in conjunction with external energy supply (Vogt and Brüning, 2013). Although our detailed understanding about food intake regulatory neurocircuits has rapidly evolved over the last years (Gautron et al., 2015; Betley et al., 2013; Carter et al., 2013; Wu et al., 2012), how the CNS controls peripheral glucose metabolism is less well defined. Recent experiments largely derived from animals with chronically altered leptin and/or insulin signaling in the ARH, and particularly AgRP and POMC neurons, have substantiated a function for these neurons in controlling HGP and peripheral insulin sensitivity in the long term (Hill et al., 2010; Könner et al., 2007).

Our experiments demonstrate that both chemogenetic and optogenetic activation of AgRP neurons can acutely induce peripheral insulin resistance. While chemogenetic activation of AgRP neurons impairs both glucose tolerance and insulin sensitivity, optogenetic activation only impairs insulin sensitivity. This may stem from a quantitative difference depending on how many AgRP neurons are activated in either experimental approach, as our transgenic chemogenetic approach activates more AgRP neurons compared to unilateral laser stimulation in the ARH of

$ChR2^{AgRP}$ mice. Alternatively, differences in the genetic background (C57bl6 for $hMD3_{Gq}^{AgRP}$ mice and C57bl6/129s for $ChR2^{AgRP}$ mice as well as their respective controls) may also account for the phenotypical difference between the chemo- and optogenetic model with respect to glucose tolerance despite them showing the same phenotype for food intake, ITT, and BAT gene expression. Nevertheless, the fact that unilateral AgRP neuron stimulation alone is sufficient to promote systemic insulin resistance points to the dominant nature of this pathway in controlling glucose homeostasis. Thus, we reveal an important regulatory principle in the physiological control of fuel fluxes, since AgRP neurons are the most effective hunger-communicating cells and therefore provide an ideal effector to impair peripheral glucose deposition in the short term, at times when external energy sources are limited.

The fact that no acute glucose regulatory effect is observed during the same time course following POMC neuron activation indicates that this short-term glucose regulatory effect governed by AgRP neurons may be AgRP- and MC4R-independent. Similarly, the acute orexigenic effects of AgRP neuron activation is mainly melanocortin-independent as acute optogenetic stimulation of AgRP neurons in *Ay* mice does not impair light-evoked feeding (Aponte et al., 2011). AgRP neurons co-express NPY as well as the inhibitory neurotransmitter GABA, both of which specifically contribute to the short-term feeding regulatory function of AgRP neurons (Krashes et al., 2013). Thus, further studies will have to clearly establish which neuropeptides or neurotransmitters mediate the acute glucose regulatory function of AgRP neurons.

In addition to the possibility that AgRP neuron-dependent acute regulation of systemic insulin sensitivity is independent of melanocortin signaling, the difference between CNO-induced activation of AgRP and POMC neurons may also stem from a fundamental difference in the architecture of AgRP and POMC neuron circuits. Recent studies from Atasoy et al. (2014) revealed a different innervation pattern of AgRP and POMC neuron projections in the PVH. AgRP projections densely target the soma of PVH neurons, while POMC projections primarily innervate the dendrites of these PVH neurons, indicating that while AgRP neurons potently control firing of downstream targets, POMC neurons may provide a more modulatory effect on the same targets. Whether this differential output organization also holds true for the glucose regulatory AgRP projection sites identified in the current study will have to be investigated in upcoming experiments.

Interestingly, while most of the models with chronically altered leptin and insulin signaling in AgRP neurons manifested with an impairment of insulin's ability to suppress HGP, insulin still fully suppressed HGP in the short term in our present model of acute AgRP neuron activation. Thus, overt de-regulation of HGP by altered AgRP neuron activity requires additional long-term, likely MC4R-mediated signals, as suggested from our experiments or by re-constituting MC4R expression in the brainstem (Berglund et al., 2014).

On the other hand, the acute and profound effect of AgRP-dependent impairment of systemic insulin sensitivity results from inhibition of insulin-stimulated glucose uptake into BAT. Again, the absence of altered BAT glucose uptake in POMC-activated mice suggests a MC4R-independent mechanism for this acute effect, in addition to the documented chronic effect of MC4R re-expression in the LHA on BAT glucose uptake (Morgan et al., 2015).

Another key finding of the present study is how rapidly, within only 1 hr of AgRP neuron activation, the transcriptional signature of BAT is altered toward a coordinated upregulation of mRNAs, which are characterized as myocyte-specific genes. These findings indicate that even in BAT of adult mice, a characteristic skeletal muscle transcriptional program can be established within short time of activating AgRP neurons. Among the muscle-specific transcripts upregulated in response to AgRP neuron activation, myostatin stood out, both by the degree of upregulation upon activation of AgRP neurons and by its previously documented role in BAT differentiation and function. Importantly, myostatin expression is upregulated in obesity and myostatin-deficient mice exhibit increased muscle mass, decreased adiposity, and increased insulin sensitivity (McPherron and Lee, 2002). While the effect of myostatin deficiency may largely depend on increased muscle mass, there is evidence for a muscle-independent function of myostatin in controlling BAT differentiation and function. For example, overexpression of myostatin impairs BAT differentiation in vitro and predadipocytes from myostatin-deficient mice exhibit an increased propensity to differentiate into brown adipocytes (Braga et al., 2013). Moreover, blockade of the myostatin receptor activin receptor IIb activates functional brown adipogenesis and thermogenesis (Fournier et al., 2012). Of note, in the gene expression analysis presented here, thermogenic genes were not dysregulated despite a clear reduction in sympathetic nerve activity following AgRP neuron activation. One explanation for this could be that these genes may follow a different time course of regulation.

Finally, we demonstrate that in cultured brown adipocytes myostatin can inhibit insulin-induced AKT activation. More importantly, our in vivo experiments reveal that acute pharmacological blockade of myostatin attenuates the ability of activated AgRP neurons to cause insulin resistance. Clearly, our experiments define myostatin as an attractive target for obesity-associated insulin resistance, as it may develop in part as a consequence of altered AgRP neuron function.

In addition to the identification of mechanisms responsible for AgRP neuron-dependent instatement of insulin resistance in peripheral tissues, our experiments define key projection sites within the CNS, which mediate AgRP neuron-dependent insulin resistance as the $aBNST_{vl}$ and the LHA. While previous studies have already linked the activity of neurons in the LHA to the control of BAT function through control of sympathetic innervation of this tissue (Morgan et al., 2015), to our knowledge, no data exist so far regarding a role for the aBNST in control of BAT function. Interestingly, using elegant approaches based on rabies virus tracing, Betley et al. (2013) identified the aBNST and PVH as the AgRP neuron projection sites innervated by the largest number of AgRP neurons, with 18.3% of AgRP neurons projecting to the BNST. Regarding the aBNST neurons responsible for mediating the ability of activated AgRP neurons to cause insulin resistance, we identified them as being located predominantly in the $aBNST_{vl}$. With respect to the efferent structures targeted by the aBNST, studies have already revealed a plethora of efferences

arising from this nucleus and innervating both structures related to control of autonomic responses as well as ingestive behavior (Dong and Swanson, 2006). Thus, our study clearly indicates a functional compartmentalization between these parts of the aBNST in terms of regulating food intake and those controlling autonomic responses. Clearly, further studies are needed to reveal the exact molecular identity of aBNST neurons in control of BAT function as well as the downstream circuitries targeted by these cells. Similarly, experiments investigating the nature of synaptic connections from AgRP neurons onto BNST neurons will be required to address whether the effects reported here are mediated by direct monosynaptic contacts or stimulation of AgRP-fibers traveling in very close proximity to the regions probed.

Finally, although we have not investigated other potential AgRP neuron projections sites in control of systemic insulin sensitivity to the full extent, the difference in the complexity of neurocircuits involved in control of feeding behavior compared to the relatively simple architecture of those in control of peripheral insulin sensitivity is obvious. This is reasonable in light of the complex behaviors that have to be integrated in the control of feeding, including assessing the nature of the food-containing environment, assigning a rewarding value to food, and finally, not only adapting autonomic responses to substrate availability but also to coordinate locomotor activity and foraging behavior.

Taken together, our experiments reveal the basic architecture for short-term control of peripheral insulin sensitivity governed by the key nutrient communicating AgRP neurons. Further defining the targets of the AgRP → LHA and AgRP → $aBNST_{vl}$ circuits as well as their effectors in BAT, such as myostatin, in control of peripheral insulin sensitivity thus may allow to define novel targets for the improvement of glucose homeostasis in subjects suffering from obesity and obesity-associated insulin resistance.

EXPERIMENTAL PROCEDURES

Animal Care

All animal procedures were conducted in compliance with protocols approved by local government authorities (Bezirksregierung Köln) and were in accordance with NIH guidelines. Mice were housed at 22°C–24°C using a 12-hr light/12-hr dark cycle. Animals had ad libitum access to water at all times, and food was only withdrawn if required for an experiment. All experiments have been performed in adult mice.

Genetic Mouse Models

Generation of ROSA26CAGSloxSTOPloxhMD3$_{Gq}$ mice is described in the Supplemental Experimental Procedures. All other mice used in this study have been previously described: AgRP-IRES-Cre (AgRP^{Cre}) (Tong et al., 2008), POMC-Cre (Balthasar et al., 2004), tdTomato reporter (B6;129S6-Gt(ROSA)26Sor$^{tm9(CAG-tdTomato)Hze}$/J (Madisen et al., 2010), and B6;129S-Gt(ROSA)26Sor$^{tm32(CAG-COP4*ChR2(H134R)EYFP)}$ Ai32; (Madisen et al., 2012) .

CNO Administration

Clozapine-N-oxide (CNO; Sigma) was injected intraperitoneally (i.p.) at a dose of 0.3 mg/kg BW unless stated differently.

Photostimulation and Calcium Imaging Photometry

Photostimulation and calcium imaging photometry were performed as previously described (Betley et al., 2013; Chen et al., 2015). For detailed experimental procedures, see the Supplemental Experimental Procedures.

Anti-myostatin Blockade and β3-Adrenergic Stimulation

Twelve hours prior to the ITT, subcutaneous (s.c.) injections of 5 mg/kg BW control IgG or anti-myostatin antibody (LSN2478185) were performed as previously described (Smith et al., 2015). The selective β3-adrenergic sympathomimetic drug CL 316,243 hydrate (1 mg/kg BW) or vehicle (saline) was co-administered together with CNO 20 min prior to the ITT.

Sympathetic Nerve Activity Recording

Sympathetic nerve activity (SNA) subserving brown adipose tissue (BAT) was recorded as previously described (Tovar et al., 2013).

Positron Emission Tomography Scans

PET imaging was performed using tail vein administration of [18F]FDG following i.p. CNO administration in anesthetized mice. For detailed description please refer to the Supplemental Experimental Procedures.

Electrophysiology

Perforated patch recordings were performed on brain slices from hM3D$_{Gq}^{AgRP}$ or hM3D$_{Gq}^{POMC}$ expressing a tdTomato reporter as previously described (Klöckener et al., 2011). For detailed information, see the Supplemental Experimental Procedures.

Statistical Analyses

All values are expressed as the mean ± SEM. Statistical analyses were conducted using GraphPad PRISM (version 5.0a). Data recorded from an animal subjected to two different treatments (CNO versus vehicle) were analyzed for statistical significance using a paired two-tailed Student's t test. Datasets with only two independent groups were analyzed for statistical significance using an unpaired two-tailed Student's t test, unless indicated otherwise in the figure legends. Datasets with more than two groups were analyzed using one-way ANOVA followed by Newman-Keuls post hoc test. Datasets subjected to two independent factors were analyzed using two-way ANOVA followed by Bonferroni post hoc test. All p values ≤ 0.05 were considered significant ($^*p \leq 0.05$, $^{**}p \leq 0.01$ and $^{***}p \leq 0.001$).

ACCESSION NUMBERS

The accession number for the microarray data reported in this paper is GEO: GSE77766. Please refer to http://www.ncbi.nlm.nih.gov/geo/info/linking.html.

SUPPLEMENTAL INFORMATION

Supplemental Information includes Supplemental Experimental Procedures, seven figures, and two tables and can be found with this article online at http://dx.doi.org/10.1016/j.cell.2016.02.044.

AUTHOR CONTRIBUTIONS

S.M.S. and J.R. contributed equally to this work. S.M.S., J.R., and J.C.B. conceived the project, designed the experiments, analyzed the data, and wrote the manuscript with input from the other authors. S.M.S. and J.R. performed all the experiments apart from: insulin-signaling in vitro (I.K.); experiments with hM3D$_{Gq}^{POMC}$-mice (I.K. and M.C.V.); in vivo calcium imaging photometry (E.T. and M.E.H.); BAT SNA experiments (D.A.M. and K.R.), and electrophysiological recordings (L.P., S.B., A.C.K., and P.K.). L.E.R. contributed to immunohistochemistry and image analysis. K.T. and E.T. performed clamps surgeries. J.M. was involved in clamps. M.E.H. configured the optogenetic and photometry infrastructures. H.B. supervised the PET-experiment. P.F. and I.K. analyzed microarray data. P.T.B., T.B., and T.F.W. generated and provided the hM3D$_{Gq}$ mouse.

ACKNOWLEDGMENTS

We are grateful to Eli Lilly and company for providing control- and anti-myostatin antibodies. We acknowledge Nadine Evers, Änne Lautenschlager, and Nadine Spenrath for outstanding technical assistance. We thank Michael Dübbert

and Jan Sydow (Electronics Lab, Institute for Zoology, University of Cologne) for providing us with the laser sources used for optogenetic and Ca^{2+}-imaging experiments. This work was supported by a grant from the DFG (BR 1492/7-1) to J.C.B. and to T.B. (BE2212 and SFB635), and we received funding by the DFG within the framework of the TRR134 and within the Excellence Initiative by German Federal and State Governments (CECAD). This work was funded (in part) by the Helmholtz Alliance (Imaging and Curing Environmental Metabolic Diseases [ICEMED]) through the Initiative and Networking Fund of the Helmholtz Association. Moreover, the research leading to these results has received funding from the European Union Seventh Framework Program (FP7/2007-2013) under grant agreement 266408. K.R. is supported by the US NIH (HL084207), the American Heart Association (14EIA18860041), the University of Iowa Fraternal Order of Eagles Diabetes Research Center, and the University of Iowa Center for Hypertension Research. S.M.S. was funded by the Humboldt-Bayer program of the Alexander Von Humboldt foundation and received a grant from CECAD. J.R. was supported by a postdoctoral fellowship from the Swedish Research Council (2013-530). I.K. was supported by a long-term EMBO fellowship.

Received: September 23, 2015
Revised: January 21, 2016
Accepted: February 20, 2016
Published: March 24, 2016

REFERENCES

Alexander, G.M., Rogan, S.C., Abbas, A.I., Armbruster, B.N., Pei, Y., Allen, J.A., Nonneman, R.J., Hartmann, J., Moy, S.S., Nicolelis, M.A., et al. (2009). Remote control of neuronal activity in transgenic mice expressing evolved G protein-coupled receptors. Neuron *63*, 27–39.

Andrews, Z.B., Liu, Z.W., Walllingford, N., Erion, D.M., Borok, E., Friedman, J.M., Tschöp, M.H., Shanabrough, M., Cline, G., Shulman, G.I., et al. (2008). UCP2 mediates ghrelin's action on NPY/AgRP neurons by lowering free radicals. Nature *454*, 846–851.

Aponte, Y., Atasoy, D., and Sternson, S.M. (2011). AGRP neurons are sufficient to orchestrate feeding behavior rapidly and without training. Nat. Neurosci. *14*, 351–355.

Atasoy, D., Betley, J.N., Su, H.H., and Sternson, S.M. (2012). Deconstruction of a neural circuit for hunger. Nature *488*, 172–177.

Atasoy, D., Betley, J.N., Li, W.P., Su, H.H., Sertel, S.M., Scheffer, L.K., Simpson, J.H., Fetter, R.D., and Sternson, S.M. (2014). A genetically specified connectomics approach applied to long-range feeding regulatory circuits. Nat. Neurosci. *17*, 1830–1839.

Balthasar, N., Coppari, R., McMinn, J., Liu, S.M., Lee, C.E., Tang, V., Kenny, C.D., McGovern, R.A., Chua, S.C., Jr., Elmquist, J.K., and Lowell, B.B. (2004). Leptin receptor signaling in POMC neurons is required for normal body weight homeostasis. Neuron *42*, 983–991.

Balthasar, N., Dalgaard, L.T., Lee, C.E., Yu, J., Funahashi, H., Williams, T., Ferreira, M., Tang, V., McGovern, R.A., Kenny, C.D., et al. (2005). Divergence of melanocortin pathways in the control of food intake and energy expenditure. Cell *123*, 493–505.

Belgardt, B.F., and Brüning, J.C. (2010). CNS leptin and insulin action in the control of energy homeostasis. Ann. N Y Acad. Sci. *1212*, 97–113.

Belgardt, B.F., Mauer, J., Wunderlich, F.T., Ernst, M.B., Pal, M., Spohn, G., Brönneke, H.S., Brodesser, S., Hampel, B., Schauss, A.C., and Brüning, J.C. (2010). Hypothalamic and pituitary c-Jun N-terminal kinase 1 signaling coordinately regulates glucose metabolism. Proc. Natl. Acad. Sci. USA *107*, 6028–6033.

Berglund, E.D., Liu, T., Kong, X., Sohn, J.W., Vong, L., Deng, Z., Lee, C.E., Lee, S., Williams, K.W., Olson, D.P., et al. (2014). Melanocortin 4 receptors in autonomic neurons regulate thermogenesis and glycemia. Nat. Neurosci. *17*, 911–913.

Betley, J.N., Cao, Z.F., Ritola, K.D., and Sternson, S.M. (2013). Parallel, redundant circuit organization for homeostatic control of feeding behavior. Cell *155*, 1337–1350.

Betley, J.N., Xu, S., Cao, Z.F., Gong, R., Magnus, C.J., Yu, Y., and Sternson, S.M. (2015). Neurons for hunger and thirst transmit a negative-valence teaching signal. Nature *521*, 180–185.

Bonala, S., Lokireddy, S., McFarlane, C., Patnam, S., Sharma, M., and Kambadur, R. (2014). Myostatin induces insulin resistance via Casitas B-lineage lymphoma b (Cblb)-mediated degradation of insulin receptor substrate 1 (IRS1) protein in response to high calorie diet intake. J. Biol. Chem. *289*, 7654–7670.

Braga, M., Pervin, S., Norris, K., Bhasin, S., and Singh, R. (2013). Inhibition of in vitro and in vivo brown fat differentiation program by myostatin. Obesity (Silver Spring) *21*, 1180–1188.

Carter, M.E., Soden, M.E., Zweifel, L.S., and Palmiter, R.D. (2013). Genetic identification of a neural circuit that suppresses appetite. Nature *503*, 111–114.

Chen, Y., Lin, Y.C., Kuo, T.W., and Knight, Z.A. (2015). Sensory detection of food rapidly modulates arcuate feeding circuits. Cell *160*, 829–841.

Dietrich, M.O., Zimmer, M.R., Bober, J., and Horvath, T.L. (2015). Hypothalamic Agrp neurons drive stereotypic behaviors beyond feeding. Cell *160*, 1222–1232.

Dong, H.W., and Swanson, L.W. (2006). Projections from bed nuclei of the stria terminalis, anteromedial area: cerebral hemisphere integration of neuroendocrine, autonomic, and behavioral aspects of energy balance. J. Comp. Neurol. *494*, 142–178.

Fournier, B., Murray, B., Gutzwiller, S., Marcaletti, S., Marcellin, D., Bergling, S., Brachat, S., Persohn, E., Pierrel, E., Bombard, F., et al. (2012). Blockade of the activin receptor IIb activates functional brown adipogenesis and thermogenesis by inducing mitochondrial oxidative metabolism. Mol. Cell. Biol. *32*, 2871–2879.

Gautron, L., Elmquist, J.K., and Williams, K.W. (2015). Neural control of energy balance: translating circuits to therapies. Cell *161*, 133–145.

Gropp, E., Shanabrough, M., Borok, E., Xu, A.W., Janoschek, R., Buch, T., Plum, L., Balthasar, N., Hampel, B., Waisman, A., et al. (2005). Agouti-related peptide-expressing neurons are mandatory for feeding. Nat. Neurosci. *8*, 1289–1291.

Hill, J.W., Elias, C.F., Fukuda, M., Williams, K.W., Berglund, E.D., Holland, W.L., Cho, Y.R., Chuang, J.C., Xu, Y., Choi, M., et al. (2010). Direct insulin and leptin action on pro-opiomelanocortin neurons is required for normal glucose homeostasis and fertility. Cell Metab. *11*, 286–297.

Joly-Amado, A., Denis, R.G., Castel, J., Lacombe, A., Cansell, C., Rouch, C., Kassis, N., Dairou, J., Cani, P.D., Ventura-Clapier, R., et al. (2012). Hypothalamic AgRP-neurons control peripheral substrate utilization and nutrient partitioning. EMBO J. *31*, 4276–4288.

Kajimura, S., Seale, P., Kubota, K., Lunsford, E., Frangioni, J.V., Gygi, S.P., and Spiegelman, B.M. (2009). Initiation of myoblast to brown fat switch by a PRDM16-C/EBP-beta transcriptional complex. Nature *460*, 1154–1158.

Kim, W.K., Choi, H.R., Park, S.G., Ko, Y., Bae, K.H., and Lee, S.C. (2012). Myostatin inhibits brown adipocyte differentiation via regulation of Smad3-mediated β-catenin stabilization. Int. J. Biochem. Cell Biol. *44*, 327–334.

Kleinridders, A., Schenten, D., Könner, A.C., Belgardt, B.F., Mauer, J., Okamura, T., Wunderlich, F.T., Medzhitov, R., and Brüning, J.C. (2009). MyD88 signaling in the CNS is required for development of fatty acid-induced leptin resistance and diet-induced obesity. Cell Metab. *10*, 249–259.

Klöckener, T., Hess, S., Belgardt, B.F., Paeger, L., Verhagen, L.A., Husch, A., Sohn, J.W., Hampel, B., Dhillon, H., Zigman, J.M., et al. (2011). High-fat feeding promotes obesity via insulin receptor/PI3K-dependent inhibition of SF-1 VMH neurons. Nat. Neurosci. *14*, 911–918.

Könner, A.C., Janoschek, R., Plum, L., Jordan, S.D., Rother, E., Ma, X., Xu, C., Enriori, P., Hampel, B., Barsh, G.S., et al. (2007). Insulin action in AgRP-expressing neurons is required for suppression of hepatic glucose production. Cell Metab. *5*, 438–449.

Krashes, M.J., Koda, S., Ye, C., Rogan, S.C., Adams, A.C., Cusher, D.S., Maratos-Flier, E., Roth, B.L., and Lowell, B.B. (2011). Rapid, reversible activation of AgRP neurons drives feeding behavior in mice. J. Clin. Invest. *121*, 1424–1428.

Krashes, M.J., Shah, B.P., Koda, S., and Lowell, B.B. (2013). Rapid versus delayed stimulation of feeding by the endogenously released AgRP neuron mediators GABA, NPY, and AgRP. Cell Metab. *18*, 588–595.

Luquet, S., Perez, F.A., Hnasko, T.S., and Palmiter, R.D. (2005). NPY/AgRP neurons are essential for feeding in adult mice but can be ablated in neonates. Science *310*, 683–685.

Madisen, L., Zwingman, T.A., Sunkin, S.M., Oh, S.W., Zariwala, H.A., Gu, H., Ng, L.L., Palmiter, R.D., Hawrylycz, M.J., Jones, A.R., et al. (2010). A robust and high-throughput Cre reporting and characterization system for the whole mouse brain. Nat. Neurosci. *13*, 133–140.

Madisen, L., Mao, T., Koch, H., Zhuo, J.M., Berenyi, A., Fujisawa, S., Hsu, Y.W., Garcia, A.J., 3rd, Gu, X., Zanella, S., et al. (2012). A toolbox of Cre-dependent optogenetic transgenic mice for light-induced activation and silencing. Nat. Neurosci. *15*, 793–802.

McPherron, A.C., and Lee, S.J. (2002). Suppression of body fat accumulation in myostatin-deficient mice. J. Clin. Invest. *109*, 595–601.

Morgan, D.A., McDaniel, L.N., Yin, T., Khan, M., Jiang, J., Acevedo, M.R., Walsh, S.A., Ponto, L.L., Norris, A.W., Lutter, M., et al. (2015). Regulation of glucose tolerance and sympathetic activity by MC4R signaling in the lateral hypothalamus. Diabetes *64*, 1976–1987.

Parton, L.E., Ye, C.P., Coppari, R., Enriori, P.J., Choi, B., Zhang, C.Y., Xu, C., Vianna, C.R., Balthasar, N., Lee, C.E., et al. (2007). Glucose sensing by POMC neurons regulates glucose homeostasis and is impaired in obesity. Nature *449*, 228–232.

Plum, L., Ma, X., Hampel, B., Balthasar, N., Coppari, R., Münzberg, H., Shanabrough, M., Burdakov, D., Rother, E., Janoschek, R., et al. (2006). Enhanced PIP3 signaling in POMC neurons causes KATP channel activation and leads to diet-sensitive obesity. J. Clin. Invest. *116*, 1886–1901.

Seale, P., Bjork, B., Yang, W., Kajimura, S., Chin, S., Kuang, S., Scimè, A., Devarakonda, S., Conroe, H.M., Erdjument-Bromage, H., et al. (2008). PRDM16 controls a brown fat/skeletal muscle switch. Nature *454*, 961–967.

Smith, R.C., Cramer, M.S., Mitchell, P.J., Capen, A., Huber, L., Wang, R., Myers, L., Jones, B.E., Eastwood, B.J., Ballard, D., et al. (2015). Myostatin neutralization results in preservation of muscle mass and strength in preclinical models of tumor-induced muscle wasting. Mol. Cancer Ther. *14*, 1661–1670.

Steculorum, S.M., Paeger, L., Bremser, S., Evers, N., Hinze, Y., Idzko, M., Kloppenburg, P., and Brüning, J.C. (2015). Hypothalamic UDP increases in obesity and promotes feeding via P2Y6-dependent activation of AgRP neurons. Cell *162*, 1404–1417.

Timmons, J.A., Wennmalm, K., Larsson, O., Walden, T.B., Lassmann, T., Petrovic, N., Hamilton, D.L., Gimeno, R.E., Wahlestedt, C., Baar, K., et al. (2007). Myogenic gene expression signature establishes that brown and white adipocytes originate from distinct cell lineages. Proc. Natl. Acad. Sci. USA *104*, 4401–4406.

Tong, Q., Ye, C.P., Jones, J.E., Elmquist, J.K., and Lowell, B.B. (2008). Synaptic release of GABA by AgRP neurons is required for normal regulation of energy balance. Nat. Neurosci. *11*, 998–1000.

Tovar, S., Paeger, L., Hess, S., Morgan, D.A., Hausen, A.C., Brönneke, H.S., Hampel, B., Ackermann, P.J., Evers, N., Büning, H., et al. (2013). K(ATP)-channel-dependent regulation of catecholaminergic neurons controls BAT sympathetic nerve activity and energy homeostasis. Cell Metab. *18*, 445–455.

Tsaousidou, E., Paeger, L., Belgardt, B.F., Pal, M., Wunderlich, C.M., Brönneke, H., Collienne, U., Hampel, B., Wunderlich, F.T., Schmidt-Supprian, M., et al. (2014). Distinct roles for JNK and IKK activation in agouti-related peptide neurons in the development of obesity and insulin resistance. Cell Rep. *9*, 1495–1506.

Vogt, M.C., and Brüning, J.C. (2013). CNS insulin signaling in the control of energy homeostasis and glucose metabolism - from embryo to old age. Trends Endocrinol. Metab. *24*, 76–84.

Wu, Q., Clark, M.S., and Palmiter, R.D. (2012). Deciphering a neuronal circuit that mediates appetite. Nature *483*, 594–597.

Zhan, C., Zhou, J., Feng, Q., Zhang, J.E., Lin, S., Bao, J., Wu, P., and Luo, M. (2013). Acute and long-term suppression of feeding behavior by POMC neurons in the brainstem and hypothalamus, respectively. J. Neurosci. *33*, 3624–3632.

Zhang, C., McFarlane, C., Lokireddy, S., Bonala, S., Ge, X., Masuda, S., Gluckman, P.D., Sharma, M., and Kambadur, R. (2011). Myostatin-deficient mice exhibit reduced insulin resistance through activating the AMP-activated protein kinase signalling pathway. Diabetologia *54*, 1491–1501.